Preventing plasmon coupling between gold nanorods improves the sensitivity of photoacoustic detection of labelled stem cells *in vivo*

Joan Comenge[†*], Oihane Fragueiro[‡], Jack Sharkey[§], Arthur Taylor[§], Marie Held[†], Neal C. Burton[‖], Brian Kevin Park[§], Bettina Wilm[§], Patricia Murray[§], Mathias Brust[‡], and Raphaël Lévy[†*]

[†] Institute of Integrative Biology, University of Liverpool, Liverpool L69 7ZB, United Kingdom

[‡] Department of Chemistry, University of Liverpool, Liverpool L69 7ZD, United Kingdom

[§] Institute of Translational Medicine, University of Liverpool, Liverpool L69 3BX, United Kingdom

[‖] iThera Medical GmbH, Zielstattstrasse 13, Munich, Germany

* Address correspondence to: J.Comenge@liverpool.ac.uk, rapha@liverpool.ac.uk

ABSTRACT

Gold nanorods are excellent contrast agents for imaging technologies which rely on near infrared absorption such as multispectral optoacoustic tomography (MSOT). For cell tracking applications, the cells of interest are labelled with the contrast agent prior to injection. However, after uptake into cells by endocytosis, the confinement and high concentration in endosomes leads to plasmon band broadening and reduced absorbance. This would limit the potential of MSOT in terms of spectral processing and, consequently, sensitivity. Here, we show that steric hindrance provided by silica coating of the nanorods leads to the preservation of their spectral properties and improved photoacoustic sensitivity. This strategy allowed the detection and monitoring by MSOT of as few as 2 x 10^4 mesenchymal stem cells in mice over a period of 15 days with a high spatial resolution. Importantly, the silica-coated nanorods did not affect the viability or differentiation potential of the transplanted mesenchymal stem cells.

It has been reported that a large number of stem cell therapies fail before they can be translated to the clinic.[1] A better understanding of the fate of transplanted cells and the ability to appropriately monitor grafting efficiency in preclinical models are factors that would facilitate clinical translation.[2–4] In this context, several nanoparticle-based imaging strategies have been proposed and used for tracking cells *in vivo*.[5–7]

Multispectral Optoacoustic Tomography (MSOT) is a novel imaging technique that combines the high sensitivity of optical imaging (pmols) and the high resolution of ultrasound (~150 µm on our system).[8] This technique is based on the generation of ultrasound following absorption of light, the so-called photoacoustic effect, first described by A. Graham Bell.[9] The main advantage with respect

to other optical-based techniques is that acoustic scattering is 3 orders of magnitude less than photon scattering,[10] which enables high resolution at 4-5 cm deep into the tissue. This makes this technique a good choice for small animal imaging and for superficial or endoscopic clinical imaging. [8]

In addition MSOT uses a range of excitation wavelengths, which facilitates spectral identification of absorbers (endogenous and exogenous) within tissue. Hence, anatomical imaging and also molecular imaging are delivered. MSOT has been used to image intratumoral localisation of liposomes, [11] and to analyse biodistribution of injected micelles,[12] amongst other applications.

MSOT relies on a multiwavelength excitation and subsequent spectral processing to identify optical signatures of contrast agents. Agents with a sharp and intense absorption band in the near infrared (NIR), where endogenous absorbance is minimal, are the best choice of exogenous contrast agents.[8,13] Gold nanorods (GNRs) fulfil these requirements and have been successfully used as contrast agents for MSOT.[14,15] However, when the distance between particles becomes of the order of a few nanometres, plasmon coupling results in a dramatic change of the optical properties, namely broadening and loss of intensity of the absorbance band. [16–18] This effect is particularly pronounced after uptake by endocytosis, when GNRs are found tightly packed in intracellular vesicles. [19,20]

Thus, plasmon coupling should be avoided to fully exploit the potential of GNRs as contrast agents for MSOT. We explore here the use of silica-coating to confer steric hindrance to gold cores even under the high packing conditions found in endosomes. Silica coating of nanoparticles is a widely used approach and therefore, reliable protocols for coating GNRs with control over the shell thickness can be found in the literature.[21,22] Silica is transparent in the visible and NIR, which ensures the maintenance of the optical properties of GNRs and consequently their photoacoustic activity. Moreover, silica coating has been reported to enhance the photoacoustic signal of individual GNRs due to its higher thermal conductivity.[23] In a pioneering study, silica-coated GNRs were used to increase the labelling efficiency of GNRs in respect to uncoated GNRs.[24] This allowed the authors to monitor the injection of 8 x 10^5 labelled cells in real time by photoacoustic imaging.

Here, we first analyse systematically the effect of the silica shell thickness on the optical properties after labelling of mouse mesenchymal stem cells (MSC). The results are then applied to determine the optimal strategy to monitor *in vivo* engraftment of subcutaneously injected MSCs. Using a multispectral approach we show how the prevention of plasmon coupling greatly improves the photoacoustic signal and reduces the limits of detection, which allowed us to monitor as few as 2 x 10^4 cells for 15 days.

RESULTS AND DISCUSSION

Gold Nanorod synthesis and characterisation

GNRs were synthesised following the protocol first reported by El-Sayed's group.[25] They were characterised by TEM, Vis-NIR spectroscopy and Dynamic Light Scattering. The core size was 68.5 ± 7.0 nm length by 27.6 ± 2.7 nm width with an average aspect ratio of 2.51 ± 0.37 as measured after

TEM analysis. Longitudinal surface plasmon resonance (LSPR) of the synthesised GNRs peaks at 729 nm as measured by Vis-NIR spectroscopy (Figure 1a).

Silica coating was achieved by adapting a protocol previously described in the literature.[22] Briefly, GNRs were firstly capped with mPEG-SH (MW: 5000 Da) and transferred to ethanol. Then, TEOS was added under basic conditions to promote silica condensation onto GNRs. GNRs with silica shells of 15.6 ± 1.5 nm (GNR-Si15), 23.3 ± 2.2 nm (GNR-Si23) , and 35.0 ± 2.4 nm (GNR-Si35) were obtained after 3 consecutive silica condensation-purification steps (Figure 1). Finally, silica-coated GNRs were transferred to water before incubation with cells. The LSPR band shifted up to 14 nm after silica coating. Also, the increase of size due to silica coating resulted in an increase of absorbance at wavelengths below 650 nm due to a stronger Rayleigh scattering. This is in agreement with previous reports [22] and it confirms the absence of aggregation during the coating.

Note that colloidal stability of silica-coated GNRs was not compromised in cell culture medium as indicated by the maintenance of the plasmon band when GNRs were incubated with DMEM supplemented with serum (Supporting Information, Figure S1). As expected, a slight increase in their hydrodynamic diameter due to absorption of proteins from the medium was observed (Supporting information, Figure S2).

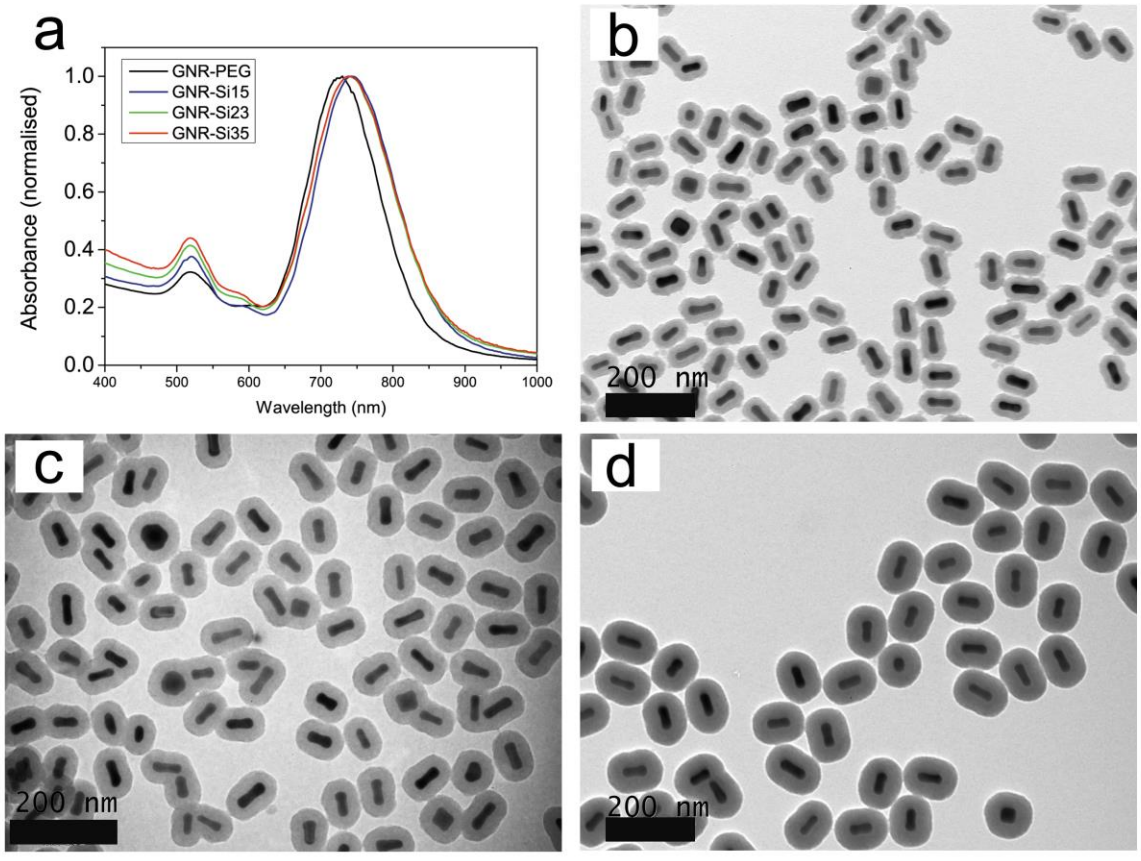

Figure 1. Characterisation of silica-coated GNRs. (a) Vis-NIR spectrum of GNRs before and after silica coating. (b-d) Representative TEM pictures of GNRs coated with 15 nm (b), 23 nm (c), and 35 nm (d) silica shells.

Labelling of mesenchymal stem cells with silica-coated GNRs

Endogenous light absorbers include molecules and proteins such as water, melanin and haemoglobin amongst others. The optical window, i.e. the region of the spectrum with lower endogenous absorbance, is in the 700 - 900 nm range (NIR).[26] Thus, to distinguish implanted cells from endogenous tissue using an optical-based technique, such as MSOT, cells need to be labelled with a contrast agent with high absorbance in the optical window. GNRs used in this work present a LSPR band between 625 and 900 nm, which makes them ideal candidates for cell labelling.

However, GNRs uptake by cells via endocytosis results in progressive accumulation of GNRs in intracellular vesicles,[27,28] which brings them in close proximity to each other. Therefore, the near-fields of neighbouring particles interact with each other, and consequently, plasmon oscillations become coupled.[16] Plasmon coupling changes the optical properties of GNRs, namely causing broadening and loss of intensity of the absorbance band.[16] Obviously, this effect would limit the potential of GNRs as probes for MSOT since this technique, as explained above, relies on a multispectral separation of the signal to distinguish the different agents. [8] Moreover, the agglomeration in the endosomes is a phenomenon that cannot be controlled, and consequently, might lead to reproducibility issues. Thus, the decrease in the absorbance would result in a lower generation of ultrasound, and the uncontrolled coupling would make multispectral unmixing difficult in complex systems such as animals where multiple endogenous absorbers are present. Altogether this would limit the potential of GNRs as MSOT probes in terms of sensitivity and spectral resolution.

Plasmon coupling strongly depends on interparticle distance.[16,18] Separations larger than 40 nm are required to minimise this effect.[29] We therefore proposed to use silica coating to sterically hinder GNR cores without affecting their inherent optical properties. To assess the efficacy of the silica shell on minimising plasmon coupling, we incubated mesenchymal stem cells (MSC) with uncoated GNRs (GNRs-PEG) as well as silica-coated GNRs with 3 different shell thicknesses (15, 23 and 35 nm). Cells were incubated with 30 pM (3.5×10^{-2} mg Au/mL) GNRs of the different preparations for 24 h. Cells were then washed, and subsequently analysed by TEM, photothermal microscopy and Vis-NIR spectroscopy.

TEM images of MSCs show GNRs entrapped in the endosomes and lysosomes. After analysis of more than 20 images per condition, we conclude that the increase in thickness of the silica shell is reflected in the distance between GNR cores in the endosomes (Figure 2). Agglomeration and even occasional sintering (gold cores fusion) were observed for uncoated GNRs (GNR-PEG). With GNRs-Si15, although no sintering was observed, the particles were packed in very close proximity to each other within the vesicles; with GNR-Si23, packing density was reduced; GNRs-Si35 remained spaced apart without any signs of closely packed gold cores. The distance between gold cores of neighbouring GNRs-Si35 in endosomes was larger than 40 nm, which should minimise any plasmon coupling effects.

It has been previously reported that silica is degraded in biological environments in a size-dependent manner.[30,31] We observed the same phenomenon: after 12 h incubation in cell culture medium, etching of the silica shell occurred in a size-dependent way (Supporting information, Figure S3). TEM images of GNRs after incubation in media show that the silica shell in GNR-Si15 is barely detectable after 12 h incubation, whilst it is still present in GNR-Si35. This is in agreement with the TEM images of labelled cells where silica coating was almost totally degraded for GNR-Si15 whilst it was

preserved, at least partially, for GNR-Si35 (Figure 2). An intermediate case is observed for GNR-Si23, with approximately half of them well isolated and the other half showing some degree of degradation. Interestingly, it has been reported that silica shell etching is not homogenous, occurring preferentially in the inner layers of silica, whilst outer layers are more resistant to etching.[32,33] This selective etching was also observed in GNR-Si23 and GNR-Si35 (Supporting Information, Figure S3) and it would explain why even if silica shells are partially degraded, they do not lose their capacity to confer steric hindrance to GNRs.

To have an overview of a broader population of cells, several 70 × 70 μm fields of view were also analysed by photothermal imaging. This technique is based on the detection of changes in the refractive index induced by conversion of the light absorbed by GNRs to thermal energy. [34] Photothermal images of several cells show a high uptake of nanorods in all cells within the field of view (Supporting Information, Figure S4). The signal presents as bright puncta throughout the cells that are several orders of magnitude brighter than the endogenous background. The localisation of the GNR signal in puncta supports the TEM-derived observation of GNRs trapped inside subcellular vesicles. In addition, imaging of several regions within a dish indicates that all cells had taken up GNRs over the course of the incubation time.

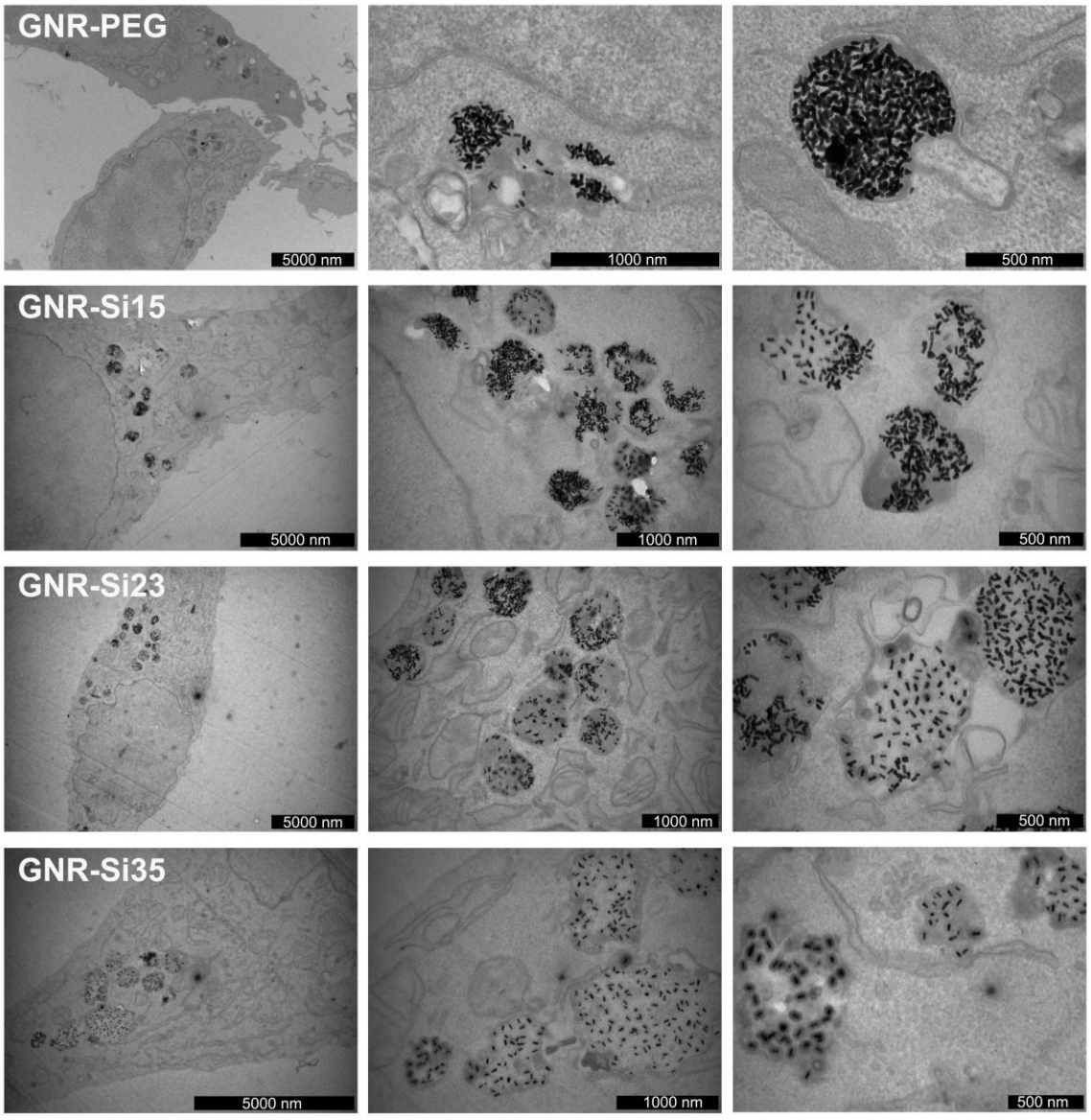

Figure 2. TEM images of GNR- labelled MSC cells. Images of cells treated with uncoated GNRs (1st row) and with silica-coated-GNRs (2nd to 4th rows). GNRs were in all cases entrapped in endosomal vesicles, but distances between the gold cores became greater as the silica shell thickness increased.

Optical properties of cells labelled under the same conditions (30 pM, 24 h) were then measured by Vis-NIR spectroscopy (Figure 3a). We observed that the spectrum of cells incubated with uncoated GNRs had a broad LSPR band with very low absorbance in the 700-900 nm range due to plasmon coupling and agglomeration as explained above. By contrast, the optical signature of GNRs was better preserved after silica coating. This preservation of the optical properties improved with increasing thickness of the silica shell. In fact, the shape of the LSPR for GNR-Si35-labelled cells was barely discernible from GNRs in solution. Interestingly, when the packing of the endosomes was disrupted by lysing cells with ultrasound, the optical properties were partially recovered (Figure 3b). In the cell lysates, GNRs were not constrained to the endosomes anymore and since most of them were not irreversibly aggregated (no fusion of gold cores), they were fully dispersed. Hence, we

conclude that the observed loss of plasmon band shape and absorbance can be attributed to the tight packing of GNRs in vesicles.

As mentioned above, we observed a partial etching of the silica shells when incubating GNRs in cell medium. However, optical properties were maintained once GNRs had been taken up, suggesting that silica etching seemed to be quenched after cell internalisation. To confirm this point on a longer timescale, cells labelled with GNR-Si35 were treated with 20 µg/mL mytomicin C for 4 h to arrest cell division[35] and kept in culture for 7 days. TEM of cells shows that silica shells were still present after 7 days and particles appeared to be well separated (Figure 4a).Optical properties of the GNRs were preserved and no significant plasmon coupling was observed in their Vis-NIR spectra (Figure 4b) An additional experiment in which cell division was not arrested supports this conclusion (Supporting Information, Figure S5). Note also that photoacoustic spectra of subcutaneously injected cells remains constant for 15 days (see below in Figure 12)

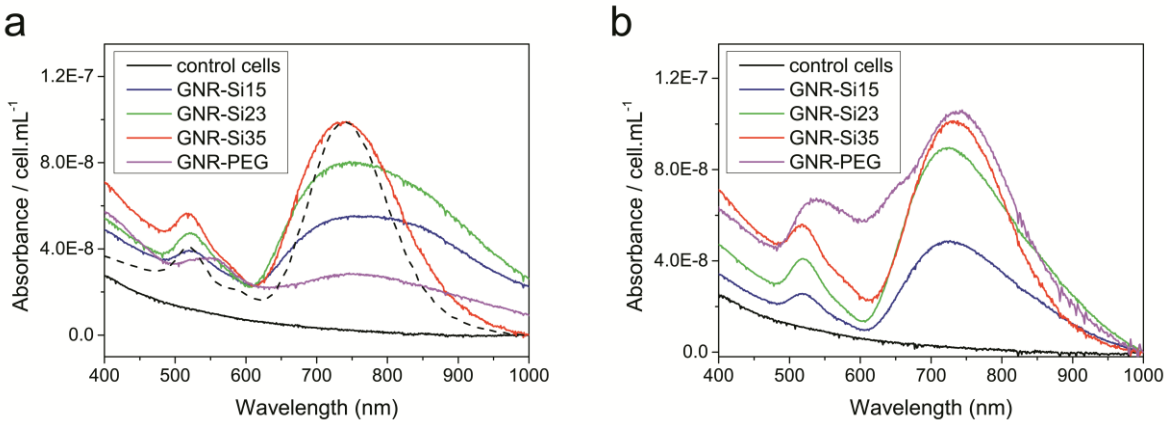

Figure 3. Optical properties of GNR-labelled cells. (a) Vis-NIR spectra of labelled cells showing the efficiency of silica in preventing plasmon coupling after cell uptake. Dashed line shows the shape of the spectra of GNR-Si35 in water to demonstrate the maintenance of optical properties of GNRs inside cells. (b) Cells measured in (a) were sonicated to show that the broadening of the peak was partially reversible after cell lysis. A dramatic change in shape and intensity was observed for the uncoated GNRs, whilst a narrowing of the band can be also appreciated for GNR-Si15 and GNR-Si23. Spectra were offset at 610 nm (a) and 1000 nm (b) to facilitate comparison.

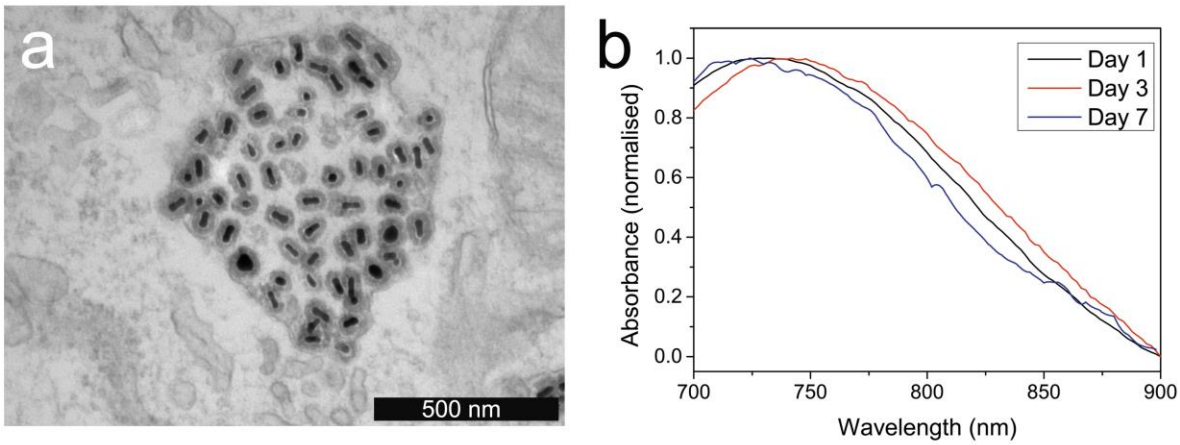

Figure 4. Stability of silica shell in cells. (a) Representative TEM image of a cell vesicle 7 days after labelling with GNR-Si35. Silica shell remains stable after cell internalisation, which is translated to maintenance of their optical properties (b).

We next investigated the relationship between intracellular concentration, optical properties and cell viability and proliferation following labelling of MSCs with GNR-Si35. Thus, we assessed in parallel the effect of GNR-Si35 concentrations on labelling efficiency, cell viability and cell proliferation. MSCs were incubated for 24 h using a range of GNR-Si35 concentrations up to 100 pM. The Vis-NIR spectra of the labelled cells (Figure 5) indicated that whilst absorbance increased with concentration, both the peak position and the shape of the LSPR band were maintained even at the highest concentration tested (100 pM). Thus, the optical signature was preserved also in cells that had taken up a greater number of GNRs. The preservation of optical properties enables the approximate number of GNRs per cell to be estimated. Hence, 1.0×10^4 GNR-Si35 per cell were calculated for the labelling concentration used here (30 pM) considering an extinction factor of 5.8×10^9 M^{-1} cm^{-1} as reported in the literature for GNRs with the same LSPR.[36]

Cell viability based on the quantification of the total amount of ATP indicated that 96 ± 1 % of the cells survived at GNRs-Si35 concentration of 30 pM when compared to the control (Figure 6a). Incubating the cells with 100 pM GNR-Si35 led to a cell viability of 87 ± 3 %. Similar trends were observed when assessing the viability 24, 48, and 72 hours after incubation (Supporting Information, Figure S6). In addition, cell proliferation assay up to 72 hours after labelling also confirmed a lack of toxicity of GNR-Si35 at the labelling conditions (Figure 6b). Therefore, GNR-Si35 showed the most interesting optical properties (*i.e.* preservation of optical signature and high absorbance in the NIR) and were not overly toxic to cells at the labelling concentration used in this work (30 pM). Thus, we decided to progress with these particles to *in vivo* imaging with MSOT.

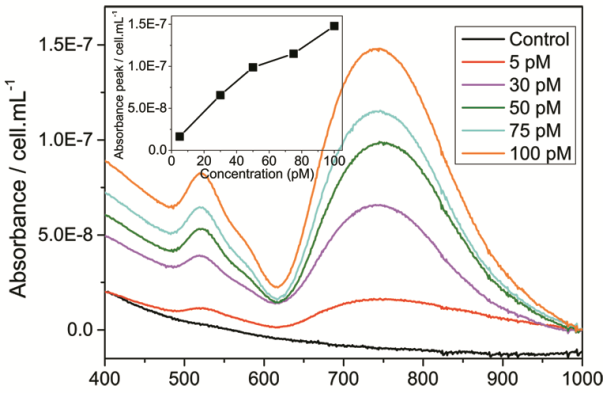

Figure 5. Effect of increasing GNRs concentration on optical stability and viability. (a) Vis-NIR spectra of cells after incubation with GNR-Si35 at different concentrations ranging from 5 to 100 pM. Spectra were offset at 1000 nm to facilitate comparison

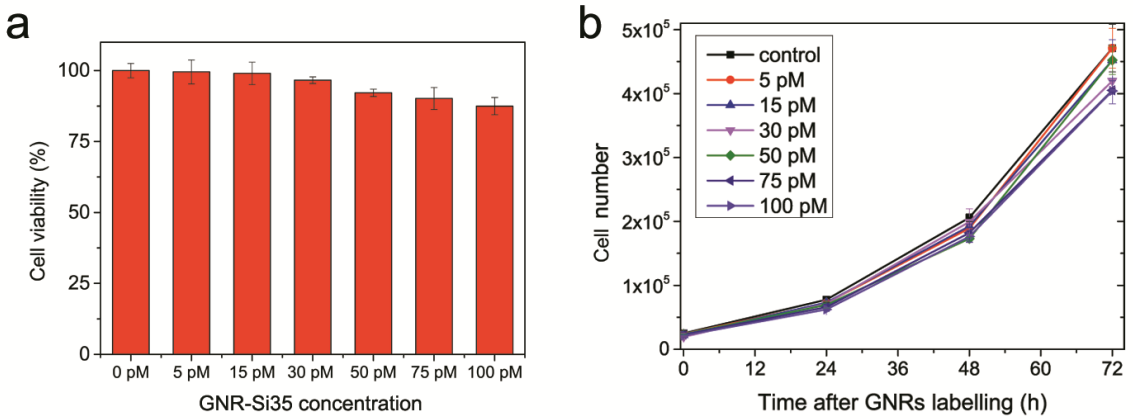

Figure 6. Cell viability and proliferation after GNR-Si35 labelling. (a) Cell viability after labelling with GNR-Si35 at different concentrations ranging from 5 to 100 pM. (b) Cell proliferation at 0, 24, 48, and 72 hours after labelling with GNR-Si35.

MSOT imaging of cells in phantoms

MSOT relies on resolving distinct multispectral signatures to detect which components are present in a specific area or region of interest (ROI). Thus, an increase of MSOT intensity is expected at the wavelengths where a specific contrast agent absorbs light. Subsequently, multispectral unmixing algorithms can be applied and correlated with the presence of components with a distinct optical signature. Before imaging labelled cells in complex systems with multiple absorbers such as animal tissues, we established in a phantom that the MSOT spectrum of GNR-Si35-labelled cells correlates with the measured ViS-NIR absorbance spectrum. To achieve this, we placed 1.5 x 10^3 cells/µL (GNRs-Si35-labelled and control MSCs) into an agar phantom and recorded MSOT intensity at wavelengths ranging from 710 to 900 nm. As expected, the photoacoustic amplitude detected in the MSOT correlates with the absorbance in this range of wavelengths (Figure 7). Thus, after applying a

multispectral unmixing algorithm, labelled cells were unequivocally distinguished from unlabelled cells (Figure 7, inset). Quantification of MSOT signal after multispectral unmixing was $1.3 \times 10^4 \pm 1.0 \times 10^2$ a.u. for GNR-labelled cells whilst it was only $8.0 \times 10^2 \pm 10$ a.u. for unlabelled cells.

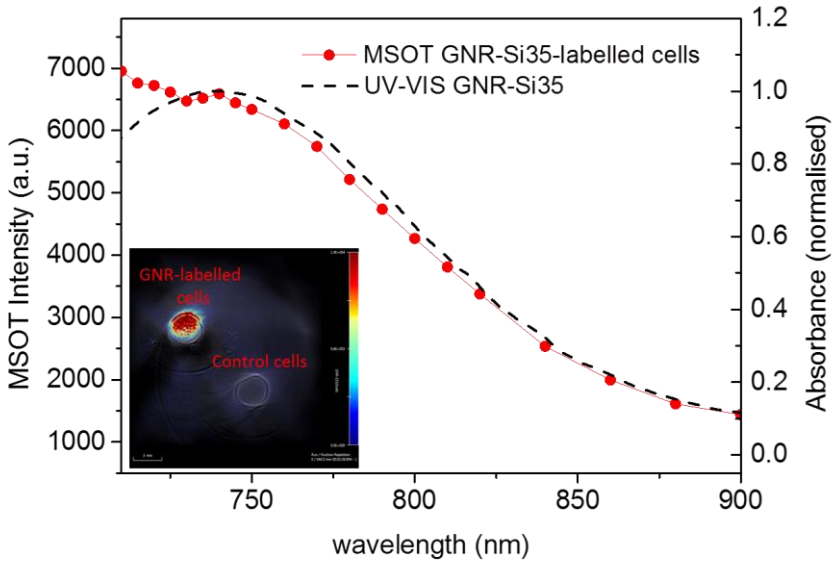

Figure 7. MSOT imaging of labelled cells in phantoms. Correlation between MSOT intensity signal of GNR-Si35 labelled cells and Vis-NIR spectra of GNRs-Si35. Inset, MSOT reconstruction image of a transversal slice of the phantom after applying multispectral processing demonstrates clear distinction between labelled and unlabelled cells. Colour scale range is 0 to 1.5×10^4 MSOT a.u.

In vivo MSOT monitoring of subcutaneously implanted mesenchymal stem cells

To demonstrate the potential of GNR-Si35 for cell tracking, 2×10^4, 1×10^5, and 2×10^5 GNR-Si35-labelled (30 pM) MSCs, as well as 2×10^5 control cells (unlabelled MSCs) were subcutaneously injected at 4 different positions into the flank of a mouse, and monitored for up to 15 days. Scans of the mouse flank from shoulder to hind leg were acquired with 0.5 mm steps at day 1, and scans of the regions of interest (*i.e.* cell clusters) were acquired with 0.3 mm steps at day 3, 5, 10 and 15. Note that reconstruction algorithms as well as MSOT intensity colour scales are the same in all *in vivo* experiments presented in this work.

GNR-Si35-labelled cells can be easily identified due to their high photoacoustic signal even at a single wavelength, in this case 760 nm (Figure 8, and Figure 9). In addition, the photoacoustic spectral signature of labelled cells was maintained after subcutaneous implantation as shown by plotting the MSOT intensity against wavelength of the region where cells were injected (Figure 8). A maximum intensity in the region of 720-740 nm, followed by a progressive decrease until 910 nm was observed only in the regions where labelled cells had been injected, which correlated with the absorbance spectra of GNR-Si35. It is of particular importance to achieve a unique optical signature with the GNR-labelled cells in order to distinguish the signal of interest from regions with high endogenous absorbance, such as the spleen. A single wavelength approach may lead to a misinterpretation of the

presence of a specific probe but this is easily solved after multispectral processing if the ROI show a distinct photoacoustic profile. This is illustrated in figure 9: single wavelength cross sections (Figure 9, left column) show the great anatomical resolution of MSOT imaging, resolving even small structures such as the renal veins and arteries. However, it is difficult to distinguish GNR-labelled cells from other regions with high photoacoustic signal. On the other hand, cells are unequivocally distinguished from any other region after multispectral processing (Figure 9, middle column). The very high signal to noise ratio enabled the monitoring of the different cell clusters for up to 15 days (Supporting Information, Figure S8 and S9). Even the smallest cell cluster (2 x 10^4 cells) at longer time assessed here (15 days) was resolved, which highlights the enhanced sensitivity of our approach. Note that in similar approaches as many as 8 x 10^5 cells were used for short-term photoacoustic monitoring of cells.[24] In addition, maintenance of plasmon band shape should enable the potential use of GNRs with different LSPR position for the simultaneous labelling of different cell types. Finally, the rapid acquisition (100 ms/λ) allowed performing a whole animal scan, enabling a tomography of the different regions of interest (Figure 9, right column)

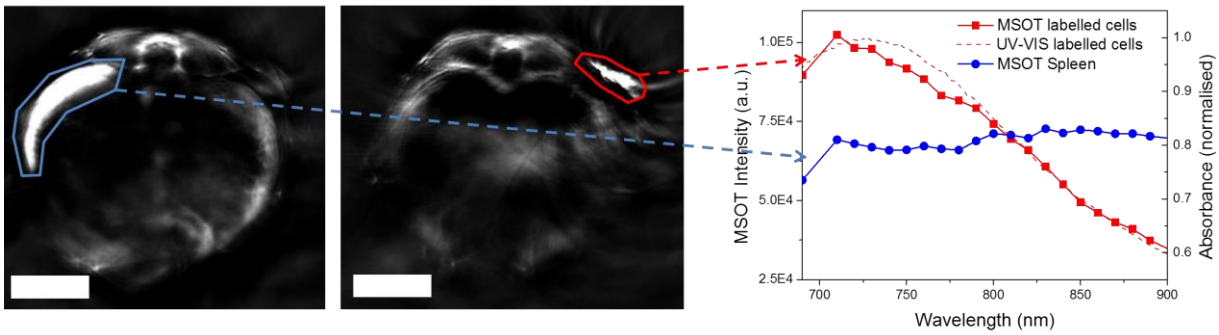

Figure 8. The importance of preserving optical properties for MSOT imaging. Cross section images of spleen (blue ROI) and GNR-Si35 labelled cells (red ROI). Both regions have strong photoacoustic intensity. However, only the photoacoustic spectrum of labelled cells fits the absorbance spectrum of GNRs which allows distinguishing the GNRs-labelled cells from any other region with high endogenous photoacoustic signal (see figure 9). Scale bars are 5 mm

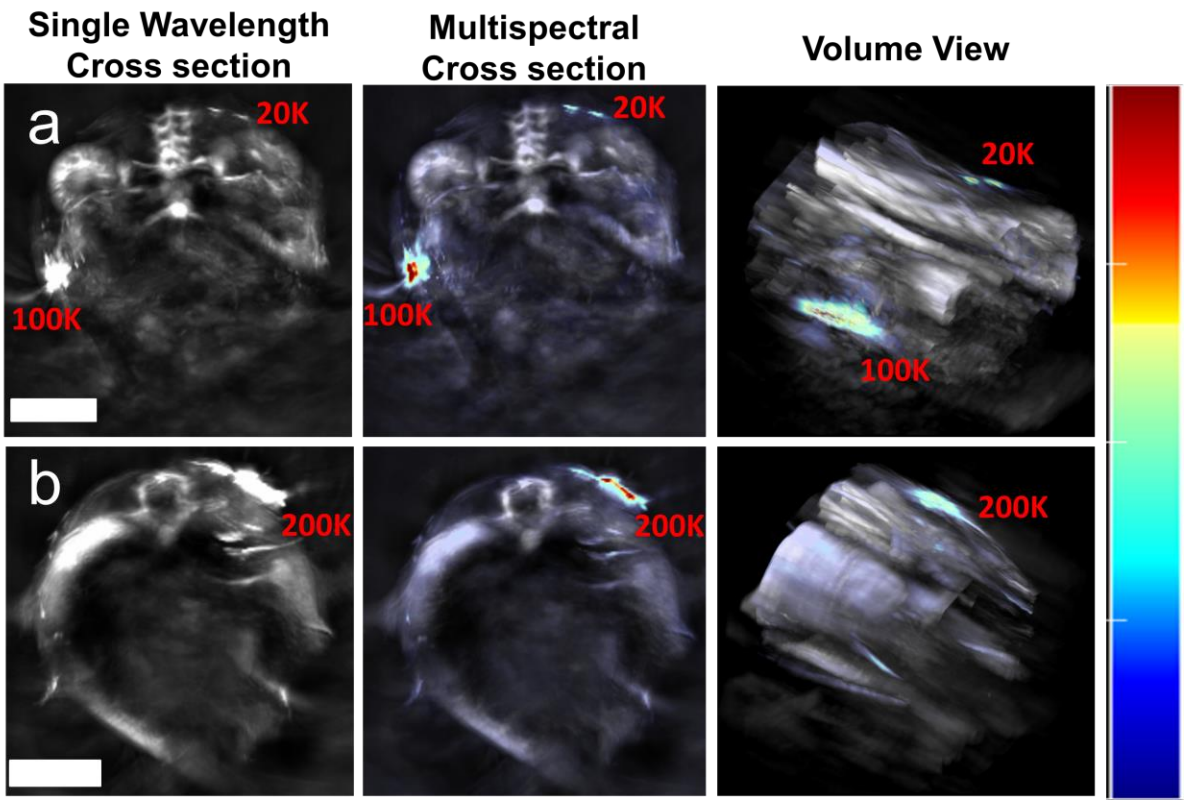

Figure 9. MSOT imaging of cell clusters. Imaging of the cell clusters 3 days after injection of 2 x 10^4 and 1 x 10^5 (a) and 2 x 10^5 GNR-Si35-labelled cells (b). The left column shows a single wavelength maximum intensity projection in the xy plane of the regions of interest. The great anatomical resolution of MSOT is observed here, allowing visualisation of small vessels (e.g. renal artery and renal vein). The middle column shows the same regions after multispectral processing, enabling high sensitivity detection of GNR-Si35 labelled cells. Volume views of the regions of interest are shown in the right column. Scale bars are 5 mm. Colour scale range is 0 to 1.1 x 10^5 MSOT a.u (same scale is used in all the *in vivo* figures)

A detailed analysis of the whole set of images after a scan of the entire mouse flank showed that control cells (i.e. unlabelled cells) and internal organs did not produce any signal of similar intensity to that of labelled cells (Supporting information, Figure S8). This is clearly visualised in a 3D image obtained after stacking the multispectral reconstruction slices of a complete scan 3 days after injection (Figure 10 and 360^o animation in supporting information). Note that the background layer (i.e. images corresponding to wavelength = 860 nm) was made transparent to facilitate the visualisation of the multispectral reconstruction and of any potential interference of endogenous absorbers. MSCs used in this work were modified to express luciferase so that bioluminescence imaging could be used to validate the *in vivo* MSOT data (Figure 10). Our bimodal imaging approach confirmed that the MSOT signal originates from the different cell clusters. Importantly, the bioluminescence signal can only be generated by living cells, which confirmed that GNR-Si35 were not affecting cell viability. In addition, a time course analysis of bioluminescence from the different cell clusters indicated that GNR-Si35 did not affect the proliferation of MSCs, as they grew exponentially after day 5 (Supporting Information, Figures S9 and S10), in agreement with previous studies on the subcutaneous injection of MSCs. [37]

Bioluminescence imaging is very sensitive and the signal intensity is proportional to the number of cells, [38] but its spatial resolution is limited.[8] MSOT's high spatial resolution allowed the small volume changes of a cell cluster to be monitored in three dimensions along the course of the experiment. The results are summarised in figure 11, and 360º 3D animations can be found in the supporting information. The volume of the cell cluster formed after injection of 2 x 10^5 labelled cells was 6.9, 6.0, 7.3, 19.9, and 27.7 mm^3 at day 1, 3, 5, 10, and 15, respectively, as measured with the 3D object counter plugin in ImageJ.[39] Interestingly, the arrested growth in volume during the first 3 days observed in MSOT correlates with the lag-phase in bioluminescence intensity analysis (Supporting Information, Figure S10). After day 3, one can easily observe that the cell cluster grew mainly in thickness while the width and length remained relatively stable. The thickness increased from 0.4 mm to 1.4 mm, length increased from 6.5 to 10 mm and width from 2.6 to 3.2 mm in the centre of the cell cluster. This represents 350% growth in depth, and 153 % and 123 % in length and width, respectively. In addition, information about the cell density can also be extracted. MSOT intensity depends on the absorbance of light and therefore on the amount of GNRs. It is observed that the intensity was higher in the core of the cell cluster immediately after injection. This trend was maintained along the time course of the experiment. Note also that the maximum intensity of the signal decreased with time. This was in agreement with the observed increase in volume since the amount of GNRs per volume unit is lower. More than the relevance of these specific values, we would like to emphasise the ability of these tools to evaluate stem cell engraftment with excellent spatial resolution and sensitivity.

Interestingly, the analysis of the photoacoustic spectra of the 2 x 10^5 cell cluster throughout the 15 days of the *in vivo* experiment revealed that no photoacoustic spectral broadening was observed, which indicates that gold cores remained isolated at least for the time of the experiment (Figure 12).

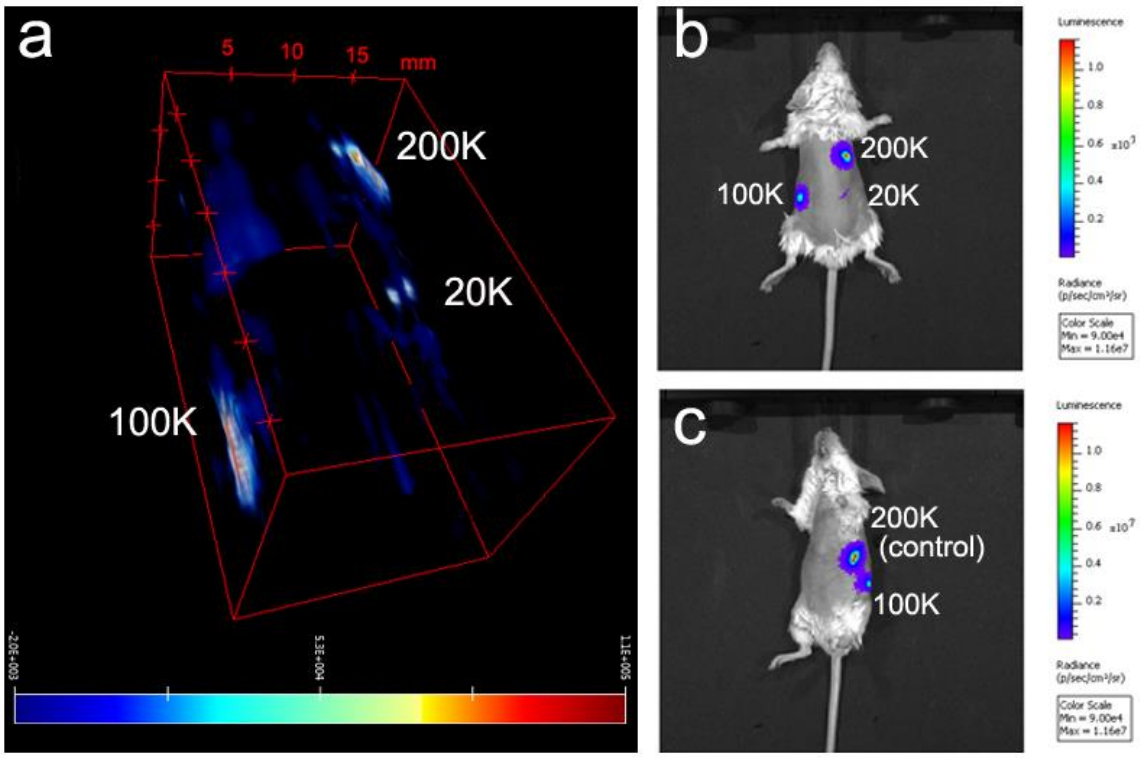

Figure 10. MSOT and bioluminescence whole animal imaging. (a) MSOT imaging of mouse flank at day 3 after subcutaneous injection. GNR-Si35-labelled cells were unequivocally distinguished from any internal organ. Scale of the box is in mm. (b) Bioluminescence imaging of the same animal. (c) Same mouse in ventral position to identify the bioluminescence signal originating from control cells.

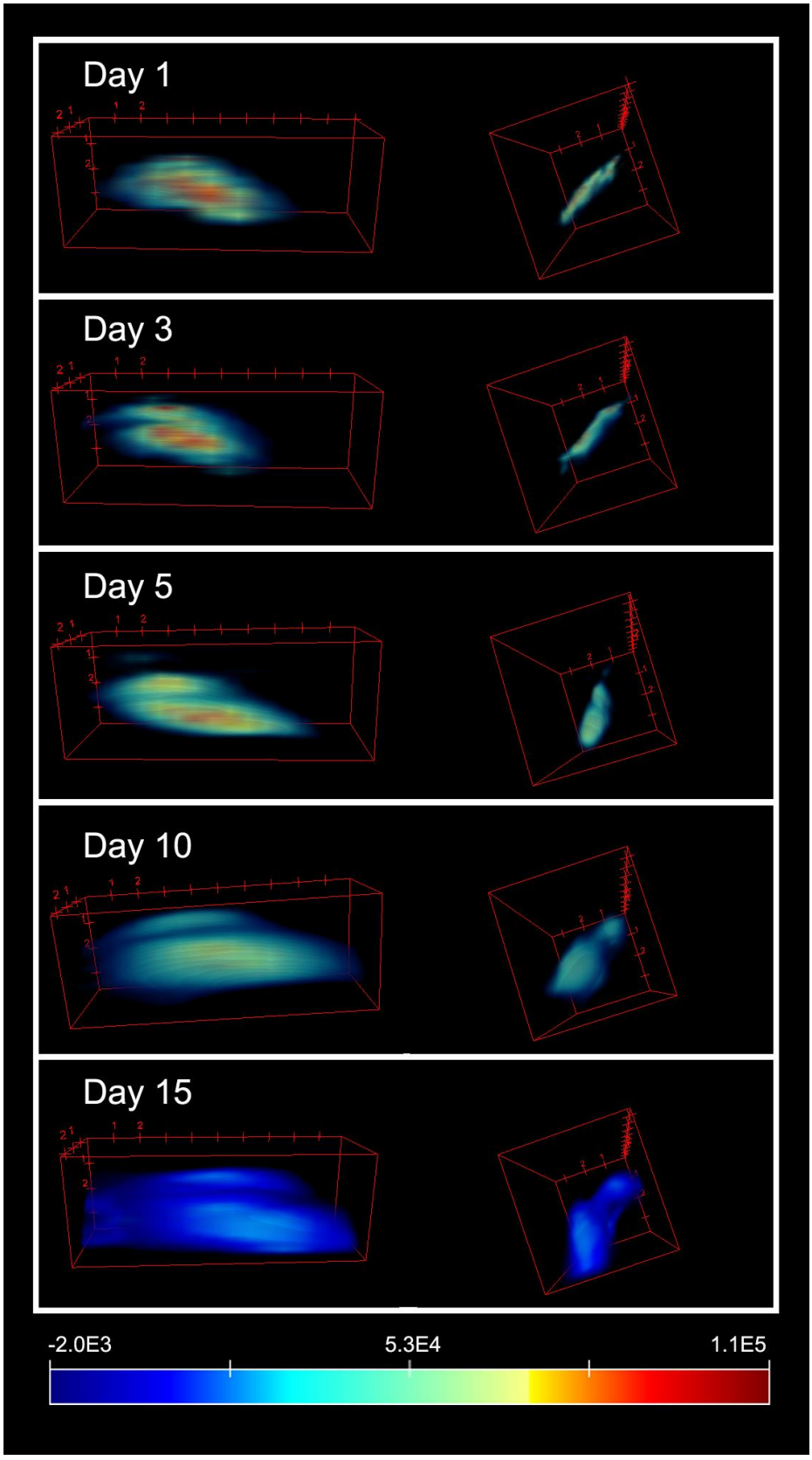

Figure 11. Monitoring the growth of the 2 x 10^5 cell cluster. Scale of the box is in mm. Note that the dimensions of all boxes are identical. Left and right columns are 90 degree rotations of the volumes shown. Colour scale is the same for all days (MSOT intensity arbitrary units).

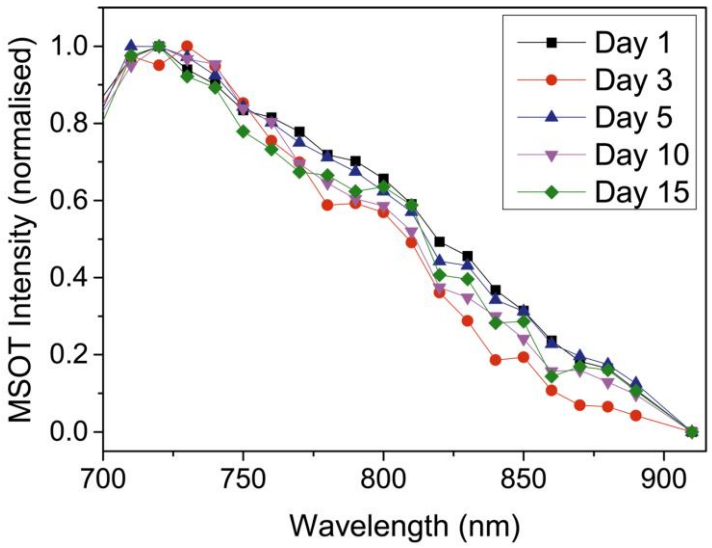

Figure 12. Photoacoustic spectra of the 2 x 10^5 cell cluster. The shape of the photoacoustic spectra was constant along the duration of the *in vivo* experiment which indicates the absence of plasmon coupling.

Finally, in similar experiments where the animals were kept for up to 19 days, we were able to identify the formation of a compact, palpable structure under the skin. Histological analysis of these structures revealed that the MSCs had differentiated into bone and cartilage (Figure 13), which is consistent with previous reports on the subcutaneous injection of this cell line in mice.[40] Therefore, our results suggest that GNR-Si35 labelling did not impair the ability of the MSCs to differentiate into different tissues *in vivo*.

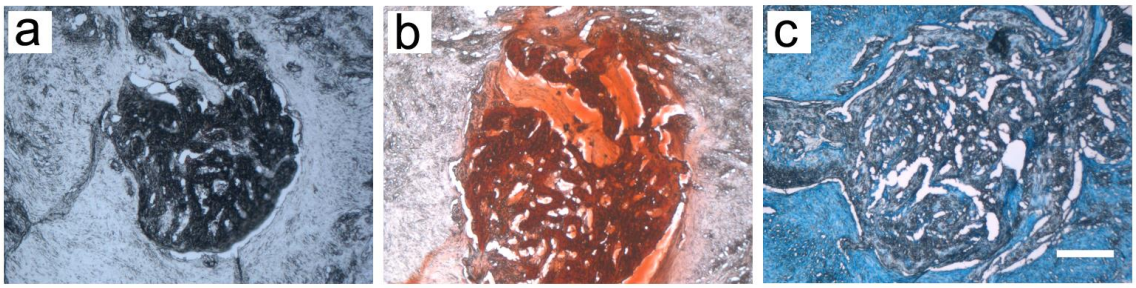

Figure 13. Histology of cell cluster formed 19 days after subcutaneous injection of 2 x 10^5 GNR-labelled cells. (a) no stain. (b) Positive staining for calcium (with alizarin red), which denotes bone formation, was found in the centre of the cell cluster. (c) Positive staining for cartilage (with alcian blue), was found in the rim of the same cell cluster. Scale bar is 200 µm.

CONCLUSIONS

In summary, we have demonstrated the importance of preventing plasmon coupling of GNRs in cells to fully exploit the potential of GNRs as NIR contrast agents. Cells retained the appealing optical properties conferred by GNRs (high absorbance and narrow plasmon band in the NIR) only when

MSCs were labelled with silica-coated GNRs. Moreover, GNRs-labelling did not affect cell viability or differentiation properties of MSCs. This was ultimately translated in a high signal *in vivo*, which allowed the monitoring of as few as 2 x 10^4 cells using MSOT, a technique that benefits from the preservation of the probe's spectral properties due to its multiwavelength acquisition approach. Interestingly, MSOT has better spatial resolution than other optical based *in vivo* imaging modalities, such as bioluminescence, without compromising the sensitivity. This allowed the 3D monitoring of a cell cluster volume growth for 15 days, with 150 µm resolution. We believe that this work can contribute to a better understanding of stem cell therapies by providing tools to precisely monitor stem cell engraftment in animal models.

MATERIALS AND METHODS

Reagents

The following chemicals were purchased from Sigma-Aldrich and used as received. $HAuCl_4 \cdot 3H_2O$ (>99.0%), $NaBH_4$ (>99.99%), $AgNO_3$(99.0%), hexadecyltrimethylammonium bromide (CTAB, >99%), L-ascorbic acid (reagent grade), tetraethyl orthosilicate (TEOS, 99.999%), O-[2-(3-Mercaptopropionylamino)ethyl]-O'-methylpolyethylene glycol (mPEG-SH, MW: 5000 Da). Monocarboxy (1-mercaptoundec-11-yl) hexaethylene glycol (PEG-COOH, MW 526.73 Da) was obtained from Prochimia.

Dulbecco's modified eagle's medium (DMEM), phosphate buffered saline (PBS), penicillin-streptomycin, alizarin red-S and alcian blue solution (1% in 3% acetic acid) were obtained from Sigma Aldrich. Foetal bovine serum (FBS) was purchased from Life-Technologies. D-Luciferin was purchased from Promega.

Cell line

The murine mesenchymal stem/stromal cell line MSC D1 (CRL-12424) was obtained from ATCC and transduced with lentiviral particles encoding a green fluorescence protein (ZsGreen) and firefly luciferase (Luc). A multiplicity of infection of 5 was used, resulting in over 95% cells expressing the transgenes. The production of viral particles and the transduction of cells was performed as previously described [41] using three plasmids encoding the viral envelope (pMD2.G), packaging proteins (psPAX2) and the transfer vector (pHIV-Luc-ZsGreen), all obtained as gifts from Didier Trono and Bryan Welm (Addgene plasmids #12259, #12260 and #39196).

Gold nanorod synthesis

GNRs were synthesised following a previously published method.[25] First, seeds were synthesised by adding 0.6 mL of ice-cold $NaBH_4$ (0.01 M) to a mixture of 5 mL CTAB (0.2 M) and 5 mL $HAuCl_4$ (0.5 mM) under vigorous stirring. The growth solution was prepared by mixing 50 mL CTAB (0.2M), 0.200 mL $AgNO_3$ (4mM), 50 mL $HAuCl_4$ (1 mM), and 0.8 mL ascorbic acid (0.1 M). Finally, 0.2 mL of freshly

synthesised seeds were added to the growth solution. The reaction was kept in a water bath at 28 °C for 3 h.

Silica coating

Silica coating was performed with slight modifications of a previously published method.[22] GNRs-CTAB underwent 2 cycles of centrifugation and resuspension with miliQ water (equal to a 625-fold purification). Then, 0.8 mL mPEG-SH (0.1 mM) were added to 50 mL GNRs solution and left for 24 h under agitation. The excess of mPEG-SH was washed off by centrifugation and the GNRs pellet was resuspended in ethanol to achieve an atomic Au concentration (as measured by the absorbance at 400 nm)[21] of 7.5 mM. Then a silica growth solution in ethanol was prepared as following: 0.5 mM atomic gold, 10.55 M water, 0.2 M ammonium hydroxide, and 0.8 mM TEOS. The reaction was kept under agitation for 2 h, followed by 2 subsequent additions of the same volume of TEOS and respective incubation steps of 2 h. The resultant GNRs had a silica shell of 15 nm. The same protocol, but using these later GNRs, was followed to obtain a silica shell of 23 nm. The same protocol was applied to further grow the silica shell to 35 nm, but using 1.2 mM TEOS instead of 0.8 mM. Silica-coated GNRs were transferred to water just before used for cell labelling. They were centrifuged and the resultant pellet resupended in water twice.

The mPEG-SH (MW: 5000 Da)-coated GNRs used for the silica growth did not show any appreciable cell uptake. Therefore, as an uncoated control, i.e. no silica shell, GNRs functionalised with PEG-COOH (MW: 526.7 Da) were used. 10 ml GNRs were purified as explained above and added dropwise in a solution of PEG-COOH (0.1 mM) in acetic acid (10 mM). The solution was kept under vigorous stirring overnight to cause reversible GNRs coagulation. Then, supernatant was removed and GNRs resuspended in a solution of PEG-COOH (0.1 mM) in NaOH (10 mM) and kept under vigorous stirring overnight. Finally, the functionalised GNRs were purified by centrifugation 3 times and resuspended in HEPES buffer (10 mM, pH 7.4).

GNRs were visualised using a Tecnai G3 spirit TEM at 120 KeV. 10 μl droplets of the sample were drop casted onto a Formvar/Carbon filmed 200-mesh copper grid (TAAB) and left to dry in air. More than 100 GNRs were considered for image analysis.

Vis-NIR spectrum was measured using Shimadzu SpectraMax Plus 384. Malvern Zetasizer nanoZS was used to measure Dynamic Light Scattering.

Cell labelling

5 x 10^5 MSCs were seeded in a 60 mm dish with 5 mL of cell culture medium (DMEM supplemented with 10% FBS). After 24 h, medium was replaced with 30 pM GNRs in fresh medium with 1% penicillin-streptomycin (80% medium + 20 % GNRs in H_2O). Cells were incubated with GNRs for 24 h. Then, cells were dissociated using trypsin, resuspended in fresh medium, washed twice with PBS and counted using an automated cell counter (TC10, BioRad).

Preparation of cells for TEM

The samples were prepared for transmission electron microscopy (TEM) using the following protocol: after 24 h incubation, cells were fixed with a solution containing 1% paraformaldehyde and 3% glutaraldehyde in 0.1 M cacodylate buffer (pH 7.4). Then, cells were incubated with a reduced osmium staining solution, containing 2% OsO_4 and 1.5% $K_4[Fe(CN)_6]$, for 1 hour. This was followed by a second 1 hour osmium staining (2% OsO_4) step and overnight staining with 1% uranyl acetate. Cells were washed with water for 3 minutes, 3 times after every staining step. Samples were then dehydrated in graded ethanol (30%, 50%, 70%, 90% and 2x 100%) for 5 minutes each. Finally, samples were infiltrated with medium TAAB resin 812 and embedded within the same resin. The resin was cured for 48 h at 60°C. Finally, ultrathin sections of 350 µm x 350 µm x 74 nm were cut and placed in 200-mesh Formvar/Carbon filmed grids. They were post-stained with uranyl acetate (4% UA in a 50:50 ethanol/water solution) and Reynolds lead citrate before TEM imaging.

Silica shell stability assays

Cells were labelled as explained above. Afterwards, cells were washed with fresh medium and treated for 4 hours with medium containing 20 µg/mL mitomycin C, followed by 3 washing steps with fresh medium. Cells were kept in the dish for 7 days and then TEM imaging was performed as explained above. Same protocol was used for Vis-NIR analysis.

Cell viability and functionality

Cell viability was assessed with Cell Titer Glo ATP Assay (Promega). Cells were labelled as described above, but seeding 10^4 MSCs cells in 96-well plates. Cells were incubated with 0, 5, 15, 30, 50, 75 and 100 pM GNRs in media (80% media and 20% GNRs solution in each case) for 24 h. After labelling, cells were washed 3 times with PBS. 50 µL of medium were added to each well and then 25 µL of the ATP reagent was added. The plate was mixed in an orbital shaker and, after 10 minutes, the contents of the plate were transferred to white, opaque, 96-well plates and the luminescence measured with a plate reader (Fluostar Omega, BMG Labtech). Each condition was assessed in triplicate and results are given as % ± SD in respect to cells that were incubated with no GNRs. The same procedure was repeated for measurements at 24, 48, and 72 h after cell labelling, but less cells were seeded before labelling to account for cell proliferation. A total of 5.0 x 10^3, 2.5 x 10^3, 1.2 x 10^3 cells were seeded respectively.

Same conditions were used for cell proliferation assay. In this case, 1.6 x 10^4 cells were seeded in 12-well plates. Cells were labelled as explained above and then the number of cells at 0, 24, 48, and 72 hours after labelling and the trypsinised and counted with an automated cell counter (TC10, Biorad).

For the migration assay, 10^4 cells were seeded in 2 well silicone insert with a defined cell-free gap (Idibi) and labelled as explained above. Then, the chamber was removed and the dishes were filled up with fresh cell culture media. Invasion of the scratch at 4 different regions was monitored for 35 hours using cell-IQ (CM Technologies). The results were expressed as % scratch closure respect to the maximum.

Animals

8 – 10 week old female BALB/c severe combined immunodeficient (SCID) mice (Charles River, Margate, UK) were housed in individually ventilated cages at a 12 hour light/dark cycle, with *ad libitum* access to food and water. Experimental animal protocols were performed in accordance with the approved guidelines under a licence granted under the Animals (Scientific Procedures) Act 1986 and approved by the University of Liverpool Animal Ethics Committee.

MSOT imaging

Animal preparation: Mice were shaved and fur epilated around the abdomen. 2 x 10^5 unlabelled MSCs, and 2 x 10^5, 1 x 10^5 and 2 x 10^4 GNR-Si35 labelled MSCs in 100 µL PBS were injected subcutaneously at 4 different positions of the mouse flank (top right, top left, bottom right and bottom left respectively). Cells were previously labelled as described above, incubating them with 30 pM GNR-Si35 for 24 h.

All imaging was performed in the inVision 256-TF MSOT imaging system (iThera Medical, Munich, Germany). For phantom imaging, 3 cross sections of the phantom were analysed using 20 different wavelengths in the range from 700 nm to 900 nm (see Figure 5). The phantom consisted of 2% agar and 1 % intralipid gel with 2 inclusions for labelled and control cells. For animal imaging, a scan of the entire mouse flank was performed with 0.5 mm steps at day 1, and of the regions of interest with 0.3 mm steps at day 3, 5, 10, 15, using 20 different wavelengths between 690 nm and 910 (see Figure 6). In all cases, linear mode based reconstruction and linear regression spectral unmixing were applied using ViewMSOT (iThera Medical).. 3D reconstructions were done by stacking 2D images with ImageJ. The 3D viewer plugin was used for the 3D image analysis.[42]

Bioluminescence imaging

Bioluminescence data was acquired using an IVIS Spectrum system (Perkin Elmer). Animals were anaesthetised with isoflurane and received a subcutaneous injection of D-luciferin (150 µg/g body weight, in PBS) 10 min prior to data acquisition. All data was analysed with Living Image (Perkin Elmer) and data is displayed in radiance units.

Histology

At the end of the experiment, the structures formed at the site of injection were harvested from the animals, fixed in 4% formaldehyde, equilibrated in 30% sucrose and cryoembedded. Tissue sections (7 µm) were obtained with a cryostat, stained with alizarin red S (2%, pH 4.3) or alcian blue and imaged using a Leica DM IL inverted microscope coupled to a DFC420C camera.

Data sets

[Comments for the attention of the referees: the DOIs below are not activated but the private hyperlinks do provide access to the data]

Full data sets associated to TEM, MSOT and photothermal images are available via Figshare at the following DOIs:

TEM of silica coated GNRs: 10.6084/m9.figshare.2055585 (15 nm), 10.6084/m9.figshare.2055591 (23 nm), 10.6084/m9.figshare.2055594 (35 nm)

TEM of labelled cells: 10.6084/m9.figshare.2055615 (PEG), 10.6084/m9.figshare.2055621 (15 nm), 10.6084/m9.figshare.2055705 (23 nm), 10.6084/m9.figshare.2055708 (35 nm)

MSOT: 10.6084/m9.figshare.2055711 (day 1), 10.6084/m9.figshare.2055717 (day 1 with background), 10.6084/m9.figshare.2055723 (day 3, all positions and wavelengths) 10.6084/m9.figshare.2055732 (day3), 10.6084/m9.figshare.2055735 (day 5), 10.6084/m9.figshare.2055744 (day 10), 10.6084/m9.figshare.2055747 (day 15)

Photothermal: 10.6084/m9.figshare.2055783 (10 pM), 10.6084/m9.figshare.2055786 (30 pM), 10.6084/m9.figshare.2055789 (control)

CONFLICT OF INTEREST

Neal C. Burton is employee of iThera Medical GmbH

ACKNOWLEDGEMENTS

This work was supported by the UK Regenerative Medicine Platform (MR/K026739/1). *In vivo* imaging data in this article were obtained in the Centre for Preclinical Imaging (CPI) of the University of Liverpool. The CPI has been funded by a Medical Research Council (MRC) grant (MR/L012707/1). Photothermal microscopy was performed in the Centre for Cell Imaging supported by MRC (MR/K015931/1).

We thank Alison Beckett (Biomedical EM Unit, University of Liverpool) for assistance and training with electron microscopy imaging of cells, Dr Marcin Grzelczack (University of Liverpool) for expert advice on silica coating protocols, and Dr Thomas Sardella and Dr Tim Devling (iThera Medical) for expert advice on MSOT imaging.

JC acknowledges the support from the People Programme (Marie Curie Actions) of the European Union's Seventh Framework Programme FP7-PEOPLE-2013-IEF under REA grant agreement n° [628809].

AUTHOR CONTRIBUTION

Conceived and designed GNRs development: JC, MB, RL. Performed GNRs development and *in vitro* experiments: JC, OF. Conceived and designed *in vivo* experiments: JC, JS, AT, PM, BW, RL. Performed MSOT and bioluminiscence imaging: JC, JS. Performed histology: AT. Performed photothermal microscopy: MH. Assisted with image analysis: NB. Contributed reagents/materials/analysis tools: BKP, BW, PM, MB, RL.

Supporting Information Available: Vis-NIR spectra, DLS, and TEM of GNRs in media, photothermal microscopy images, Vis-NIR of cells after up to 72 h, MSOT scans, and bioluminescence images and data analysis. This material is available free of charge via the Internet at http://pubs.acs.org.

REFERENCES

(1) Daley, G. Q. The Promise and Perils of Stem Cell Therapeutics. *Cell Stem Cell* **2012**, *10*, 740–749.

(2) Guzman, R.; Uchida, N.; Bliss, T. M.; He, D.; Christopherson, K. K.; Stellwagen, D.; Capela, A.; Greve, J.; Malenka, R. C.; Moseley, M. E.; *et al.* Long-Term Monitoring of Transplanted Human Neural Stem Cells in Developmental and Pathological Contexts with MRI. *Proc. Natl. Acad. Sci.* **2007**, *104* , 10211–10216.

(3) Daadi, M. M.; Li, Z.; Arac, A.; Grueter, B. a; Sofilos, M.; Malenka, R. C.; Wu, J. C.; Steinberg, G. K. Molecular and Magnetic Resonance Imaging of Human Embryonic Stem Cell-Derived Neural Stem Cell Grafts in Ischemic Rat Brain. *Mol. Ther.* **2009**, *17*, 1282–1291.

(4) de Vries, I. J. M.; Lesterhuis, W. J.; Barentsz, J. O.; Verdijk, P.; van Krieken, J. H.; Boerman, O. C.; Oyen, W. J. G.; Bonenkamp, J. J.; Boezeman, J. B.; Adema, G. J.; *et al.* Magnetic Resonance Tracking of Dendritic Cells in Melanoma Patients for Monitoring of Cellular Therapy. *Nat. Biotechnol.* **2005**, *23*, 1407–1413.

(5) Taylor, A.; Wilson, K. M.; Murray, P.; Fernig, D. G.; Lévy, R. Long-Term Tracking of Cells Using Inorganic Nanoparticles as Contrast Agents: Are We There Yet? *Chemical Society Reviews*, **2012**, *41*, 2707.

(6) Kircher, M. F.; Gambhir, S. S.; Grimm, J. Noninvasive Cell-Tracking Methods. *Nat. Rev. Clin. Oncol.* **2011**, *8*, 677–688.

(7) Meir, R.; Shamalov, K.; Betzer, O.; Motiei, M.; Horovitz-Fried, M.; Yehuda, R.; Popovtzer, A.; Popovtzer, R.; Cohen, C. J. Nanomedicine for Cancer Immunotherapy: Tracking Cancer-Specific T-Cells in Vivo with Gold Nanoparticles and CT Imaging. *ACS Nano* **2015**, *9*, 6363–6372.

(8) Ntziachristos, V.; Razansky, D. Molecular Imaging by Means of Multispectral Optoacoustic Tomography (MSOT). *Chem. Rev.* **2010**, *110*, 2783–2794.

(9) Bell, A. G. The Production of Sound by Radiant Energy. *Science.* **1881**, *os-2*, 242–253.

(10) Wang, L. V; Hu, S. Photoacoustic Tomography: In Vivo Imaging from Organelles to Organs. *Science (80-.).* **2012**, *335*, 1458–1462.

(11) Beziere, N.; Lozano, N.; Nunes, A.; Salichs, J.; Queiros, D.; Kostarelos, K.; Ntziachristos, V. Dynamic Imaging of PEGylated Indocyanine Green (ICG) Liposomes within the Tumor Microenvironment Using Multi-Spectral Optoacoustic Tomography (MSOT). *Biomaterials* **2014**, *37C*, 415–424.

(12) Sreejith, S.; Joseph, J.; Lin, M.; Menon, N. V.; Borah, P.; Ng, H. J.; Loong, Y. X.; Kang, Y.; Yu, S. W.-K.; Zhao, Y. Near-Infrared Squaraine Dye Encapsulated Micelles for in Vivo Fluorescence and Photoacoustic Bimodal Imaging. *ACS Nano* **2015**, *9*, 5695–5704.

(13) Chamberland, D. L.; Agarwal, A.; Kotov, N.; Brian Fowlkes, J.; Carson, P. L.; Wang, X. Photoacoustic Tomography of Joints Aided by an Etanercept-Conjugated Gold Nanoparticle Contrast Agent-an Ex Vivo Preliminary Rat Study. *Nanotechnology* **2008**, *19*, 095101.

(14) Taruttis, A.; Lozano, N.; Nunes, A.; Jasim, D. a; Beziere, N.; Herzog, E.; Kostarelos, K.; Ntziachristos, V. siRNA Liposome-Gold Nanorod Vectors for Multispectral Optoacoustic Tomography Theranostics. *Nanoscale* **2014**, *6*, 13451–13456.

(15) Taruttis, A.; Herzog, E.; Razansky, D.; Ntziachristos, V. Real-Time Imaging of Cardiovascular Dynamics and Circulating Gold Nanorods with Multispectral Optoacoustic Tomography. *Opt. Express* **2010**, *18*, 19592–19602.

(16) Jain, P. K.; El-Sayed, M. a. Plasmonic Coupling in Noble Metal Nanostructures. *Chem. Phys. Lett.* **2010**, *487*, 153–164.

(17) Harford, C. G.; Hamlin, A.; Parker, E. Electron Microscopy of HeLa Cells after the Ingestion of Colloidal Gold. *J. Biophys. Biochem. Cytol.* **1957**, *3*, 749–756.

(18) Sánchez-Iglesias, A.; Grzelczak, M.; Pérez-Juste, J.; Liz-Marzán, L. M. Binary Self-Assembly of Gold Nanowires with Nanospheres and Nanorods. *Angew. Chemie - Int. Ed.* **2010**, *49*, 9985–9989.

(19) Dykman, L. A.; Khlebtsov, N. G. Uptake of Engineered Gold Nanoparticles into Mammalian Cells. *Chem. Rev.* **2014**, *114*, 1258–1288.

(20) Zhang, W.; Ji, Y.; Wu, X.; Xu, H. Trafficking of Gold Nanorods in Breast Cancer Cells: Uptake, Lysosome Maturation, and Elimination. *ACS Appl. Mater. Interfaces* **2013**, *5*, 9856–9865.

(21) Pastoriza-santos, I.; Liz-marzán, L. M. Nanomaterial Interfaces in Biology. **2013**, *1025*, 75–93.

(22) Fernández-López, C.; Mateo-Mateo, C.; Alvarez-Puebla, R. a; Pérez-Juste, J.; Pastoriza-Santos, I.; Liz-Marzán, L. M. Highly Controlled Silica Coating of PEG-Capped Metal Nanoparticles and Preparation of SERS-Encoded Particles. *Langmuir* **2009**, *25*, 13894–13899.

(23) Chen, Y.-S.; Frey, W.; Kim, S.; Kruizinga, P.; Homan, K.; Emelianov, S. Silica-Coated Gold Nanorods as Photoacoustic Signal Nanoamplifiers. *Nano Lett.* **2011**, *11*, 348–354.

(24) Jokerst, J. V; Thangaraj, M.; Kempen, P. J.; Sinclair, R.; Gambhir, S. S. Photoacoustic Imaging of Mesenchymal Stem Cells in Living Mice via Silica-Coated Gold Nanorods. *ACS Nano* **2012**, 5920–5930.

(25) Nikoobakht, B.; El-sayed, M. A. Preparation and Growth Mechanism of Gold Nanorods (NRs) Using Seed-Mediated Growth Method. **2003**, 1957–1962.

(26) Weissleder, R. A Clearer Vision for in Vivo Imaging. *Nat. Biotechnol.* **2001**, *19*, 316–317.

(27) Alkilany, A. M.; Boulos, S. P.; Lohse, S. E.; Thompson, L. B.; Murphy, C. J. Homing Peptide-Conjugated Gold Nanorods : The Effect of Amino Acid Sequence Display on Nanorod Uptake and Cellular Proliferation. *Bioconjug. Chem.* **2014**, *25*, 1162–1171.

(28) Gosselin, R. E. The Uptake of Radiocolloid by Macrophages in Vitro: A Kinetic Analysis with Radioactive Colloidal Gold. *J. Gen. Physiol.* **1956**, *39*, 625–649.

(29) Funston, A. M.; Novo, C.; Davis, T. J.; Mulvaney, P. Plasmon Coupling of Gold Nanorods at Short Distances and in Different Geometries. *Nano Lett.* **2009**, *9*, 1651–1658.

(30) Cauda, V.; Schlossbauer, A.; Bein, T. Bio-Degradation Study of Colloidal Mesoporous Silica Nanoparticles: Effect of Surface Functionalization with Organo-Silanes and Poly(ethylene Glycol). *Microporous Mesoporous Mater.* **2010**, *132*, 60–71.

(31) Desai, D.; Karaman, D. Ş.; Prabhakar, N.; Tadayon, S.; Duchanoy, A.; Diana, M. Design Considerations for Mesoporous Silica Nanoparticulate Systems in Facilitating Biomedical Applications. *Mesoporous Biomater.* **2014**, *1*, 16–43.

(32) Volkert, A. a.; Pierre, M. C. S.; Shrestha, B.; Haes, A. J. Implications of Sample Aging on the Formation of Internally Etched Silica Coated Gold Nanoparticles. *RSC Adv.* **2015**, *5*, 3774–3780.

(33) Wong, Y. J.; Zhu, L.; Teo, W. S.; Tan, Y. W.; Yang, Y.; Wang, C.; Chen, H. Revisiting the Stöber Method: Inhomogeneity in Silica Shells. *J. Am. Chem. Soc.* **2011**, *133*, 11422–11425.

(34) Nieves, D. J.; Li, Y.; Fernig, D. G.; Lévy, R. Photothermal Raster Image Correlation Spectroscopy of Gold Nanoparticles in Solution and on Live Cells. *R. Soc. Open Sci.* **2015**, *2*, 140454.

(35) Sognier, M. A.; Hittelman, W. N. Mitomycin-Induced Chromatid Breaks in HeLa Cells: A Consequence of Incomplete DNA Replication. *Cancer Res.* **1986**, *46*, 4032–4040.

(36) Orendorff, C. J.; Murphy, C. J. Gold Nanorod Quantitation of Metal Content in the Silver-Assisted Growth of Gold Nanorods. *J. Phys. Chem. B* **2006**, *110*, 3990–3994.

(37) Yan, X.; Fu, C.; Chen, L.; Qin, J.; Zeng, Q.; Yuan, H.; Nan, X.; Chen, H.; Zhou, J.; Lin, Y.; *et al.* Mesenchymal Stem Cells from Primary Breast Cancer Tissue Promote Cancer Proliferation and Enhance Mammosphere Formation Partially via EGF/EGFR/Akt Pathway. *Breast Cancer Res. Treat.* **2012**, *132*, 153–164.

(38) Bednar, B.; Zhang, G.-J.; Williams Jr, D. L.; Hargreaves, R.; Sur, C. Optical Molecular Imaging in Drug Discovery and Clinical Development. *Expert Opin. Drug Discov.* **2007**, *2*, 65–85.

(39) Bolte, S.; Cordelières, F. P. A Guided Tour into Subcellular Colocalization Analysis in Light Microscopy. *J. Microsc.* **2006**, *224*, 213–232.

(40) Juffroy, O.; Noël, D.; Delanoye, A.; Viltart, O.; Wolowczuk, I.; Verwaerde, C. Subcutaneous Graft of D1 Mouse Mesenchymal Stem Cells Leads to the Formation of a Bone-like Structure. *Differentiation.* **2009**, *78*, 223–231.

(41) Pereira, S.; Moss, D.; Williams, S.; Murray, P.; Taylor, A. Overexpression of the MRI Reporter Genes Ferritin and Transferrin Receptor Affect Iron Homeostasis and Produce Limited Contrast in Mesenchymal Stem Cells. *Int. J. Mol. Sci.* **2015**, *16*, 15481–15496.

(42) Schmid, B.; Schindelin, J.; Cardona, A.; Longair, M.; Heisenberg, M. A High-Level 3D Visualization API for Java and ImageJ. *BMC Bioinformatics* **2010**, *11*, 274.

Table of Contents